JMEPEG (2002) 11:519–526

Experimental Study of the Thermal Stability of Austempered Ductile Irons

M.J. Pérez, M.M. Cisneros, E. Valdés, H. Mancha, H.A. Calderón, and R.E. Campos

(Submitted 12 April 2000)

A nonisothermal annealing was applied to austempered Ni-Cu-Mo alloyed and unalloyed ductile irons to determine the thermal stability of the ausferritic structure. Differential thermal analysis (DTA) results were used to build the corresponding stability diagrams. The transformation starting temperature of the high carbon austenite was found to be strongly dependent on the austempering temperature, the heating rate, and the chemical composition of the iron. The Ni-Cu-Mo alloying elements and high austempering temperature increased the stability. The transformation of the austenite to ferrite and cementite is achieved via the precipitation of transition carbides identified as silico-carbides of triclinic structure.

Keywords austempered ductile irons, austenite decomposition, nonisothermal annealing, thermal stability

1. Introduction

The austempering treatment in ductile irons allows the formation of an ausferritic structure consisting of a mixture of high carbon austenite (γ) and supersaturated ferrite (α) acicular phases. This microstructure results from the decomposition of the high-temperature austenite γ according to reaction I: $\gamma \rightarrow (\alpha) + (\gamma)$, which, because of the low diffusion rate of carbon, also produces carbides inside the ferrite when the reaction takes place at low austempering temperatures. The ausferrite nucleates at the graphite-austenite interface and grows throughout the eutectic cell; the intercellular regions are transformed at the end. For the austenite to remain as (γ) while cooling to room temperature requires that enough carbon be dissolved; otherwise, austenite transforms to martensite. Extended holding times at the austempering temperature encourage the high carbon austenite decomposition through reaction II: $(\alpha) + (\gamma) \rightarrow \alpha$ + carbides, causing a detrimental effect on the mechanical properties, mainly on the ductility.[1-3] Many studies[2,4-7] have been performed to determine the austempering processing window for all type of irons, which is defined as the temperature and time conditions to maximize the degree of advancement in reaction I and minimize that of reaction II. The processing conditions falling in such a window lead to optimal mechanical properties, which are given by a carbide- and martensite-free ausferritic microstructure.

An important aspect that has received less attention from researchers is the establishment of the thermal conditions for the stability of the microstructure and the mechanical properties during service. The microstructure and mechanical integrity depend on the stability of the high carbon austenite that can decompose into ferrite and carbides under given service conditions. During the tempering of austempered ductile irons (ADIs) alloyed with Mn, Chobaut et al.[8] followed the microstructure evolution. Using a dilatometric analysis, they observed a contraction at 400 °C that was associated with the high carbon austenite decomposition into ferrite and silico-carbides. They reported the presence of secondary martensite promoted by Mn. After a tempering of 216 h at 360 °C to ductile irons austempered at 380 °C, Liu et al.[9] reported the complete decomposition of the high carbon austenite. By transmission electronic microscopy (TEM) observations, they showed that the precipitation of monoclinic Hägg carbides in the austenite took place before 96 h of tempering and it was followed by the formation of the equilibrium ferrite. Using x-ray analysis, Massone et al.[10] observed the complete elimination of the high carbon austenite in a Ni-Cu ADI aged for 120 h at 360 °C. In a study performed with a differential scanning calorimeter, Korichi and Priestner[11] found that the high carbon austenite decomposed in the vicinity of 460-470 °C and observed that low austempering temperatures induced lower thermal stability of the austenite. Using dilatometric analysis to study the aging reactions in ADIs, Nadkarni and Gokhale[12] observed volumetric changes associated to the following three successive reactions: the tempering of martensite, the decomposition of high carbon austenite, and the growth of silico-carbides. They reported the austenite transformation occurring in the range of 450-550 °C.

In this work, the differential thermal analysis (DTA) was used to investigate the effect of the austempering temperature and simultaneous additions of Ni, Cu, and Mo on the thermal stability of the ausferrite in ADIs during nonisothermal annealing carried out from 300-700 °C. The microstructural changes were followed by TEM observations. Ausferrite stability diagrams were obtained for unalloyed (H1) and Ni-Cu-Mo alloyed (H2) ADIs.

2. Experimental Techniques

An unalloyed and a Ni-Cu-Mo alloyed ductile irons were produced by induction melting using the following as raw ma-

M.J. Pérez, M.M. Cisneros, and **E. Valdés,** Departamento Metal – Mecánica, Instituto Tecnológico de Saltillo, V. Carranza 2400, 25280 Saltillo Coah., México; **H. Mancha,** Cinvestav–Unidad Saltillo, Carr. Saltillo–Monterrey Km 13, 25000 Saltillo Coah., México; **H.A. Calderón,** Depto. Ciencia de Materiales, ESFM-IPN, Zacatenco Ed. 9, 07307 México D.F.; and **R.E. Campos,** Instituto de Metalurgia, Av. Sierra Leona 550, 78210 San Luis Potosí SLP, México. Contact e-mail: mmcisner@fenix.its.mx.

terials: steel scrap, ductile iron returns, ferro-silicon, and graphite. Electrolytic Ni and Cu, and ferro-molybdenum were used as alloying materials. The spheroidizing process using Fe-Si-5%Mg was performed in a Tundish-cover reactor. Inoculation in the pouring ladle was carried out by adding Fe-75%Si. The metal was poured in silica sand molds with the Y blocks impression, according to American Society for Testing and Materials (ASTM) A897M–90 specifications.

The chemical compositions of the irons are indicated in Table 1. The samples prepared from the Y blocks were aus-

Table 1 Chemical Composition of H1 and H2 Irons, wt.%

Cast Designation	C	Si	Mn	S	P	Mg	Ni	Cu	Mo
Unalloyed iron H1	3.72	2.26	0.24	0.028	0.017	0.033	…	…	…
Ni-Cu-Mo alloyed iron H2	3.66	2.23	0.26	0.015	0.024	0.047	1.02	0.66	0.26

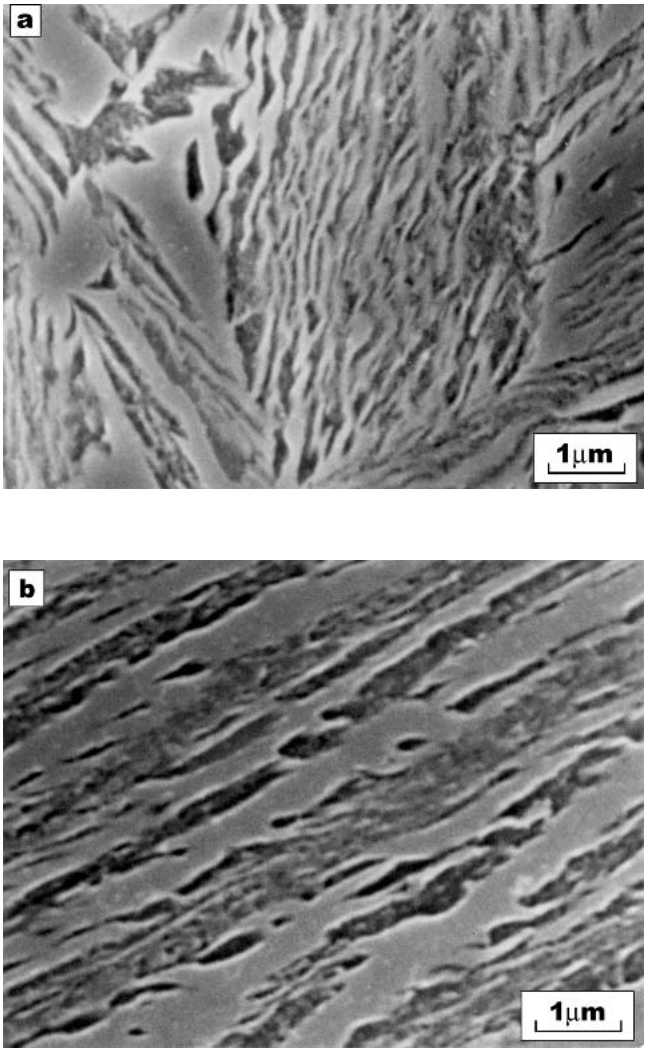

Fig. 1 SEM micrographs of H2 iron showing the ausferritic structure obtained after the austempering for 2 h at **(a)** 315 °C and **(b)** 370 °C

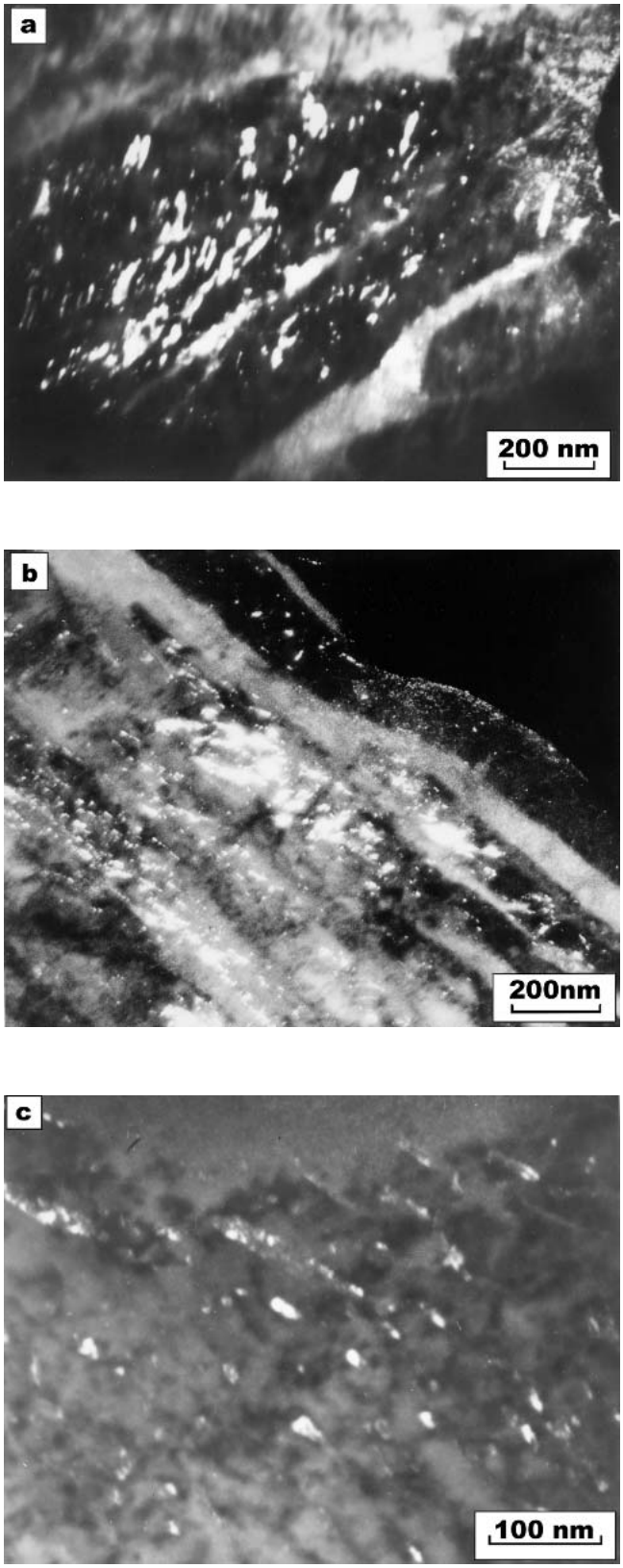

Fig. 2 Centered dark field TEM micrographs of the austempered irons showing the presence of carbides. **(a)** $(1\bar{1}1)\eta$ reflection from H1 iron (T_A = 370 °C, 2 h). **(b)** $(0\bar{1}10)\varepsilon$ reflection from H2 iron (T_A = 315 °C, 2 h). **(c)** $(\bar{4}01)\chi$ reflection from H1 iron (T_A = 315 °C, 2 h)

tenitized at 870 °C for 2 h and then austempered in a salt bath at 420, 370, 350, 315, and 270 °C for 2 h.

X-ray diffraction patterns were obtained on a X′ Pert diffractometer (Philips, Almeo, Holland) using the Cu Kα radiation (λ = 1.543 Å). From the 2θ-angle position of the austenite peaks, the lattice parameter (a_γ) of the austenite was determined and the carbon content (C_γ) was calculated using the following equation:

$$C_\gamma = \left(\frac{a_\gamma - 3.548}{0.044}\right)$$

The high carbon austenite volume fraction (X_γ) was estimated by applying the Cullity[13] direct comparison method.

A differential thermal analyzer (Stanton Redcroft, London, UK) was used to achieve the thermal study of the ausferritic microstructure. Test specimens of 200 mg were taken up to 700 °C using heating rates of 10, 20, and 30 °C/min under an argon atmosphere.

Applying a heating rate of 20 °C/min, irons austempered at 370 and 315 °C were submitted to a nonisothermal annealing at the following temperatures: 300, 400, 500, 600, and 700 °C.

Thin foils were prepared by ion milling before and after the annealing treatment from H2 iron and after the austempering treatment from H1 iron. The TEM observations were carried out in a CM 200 transmission electron microscope (Philips).

3. Results

3.1 Austempered Iron Microstructures

Figure 1 shows that 2 h of isothermal austempering at 315 and 370 °C allowed in H1 and H2 irons a martensite-free ausferritic microstructure, with thicker plates produced at the higher austempering temperature. TEM analysis revealed that in addition to the ferrite and the high carbon austenite, carbide precipitation occurred. Orthorhombic η-carbides, which precipitated inside the ferrite as well as in the α/γ interface, were found in H1 and H2 irons austempered at 370 °C (Fig. 2a). Only hexagonal ε-carbides, mainly located inside the ferrite plates (Fig. 2b) and produced by reaction I, were observed in H2 irons austempered at 315 °C. The fact that no other type of carbides appeared before 120 min of treatment is due to the decreasing kinetics of reaction I and the onset delay of reaction II caused by the alloying elements. Conversely, in unalloyed irons austempered at 315 °C (H1), the ε-carbides precipitated at short treatment times and disappeared before 120 min of treatment, whereas reaction II occurred and formed type Hägg (χ) monoclinic carbides (Fig. 2c).

Similar results for carbide precipitation have been reported in the literature: Sidjanin and Smallman[14] observed free-carbides structures during the first hour of austempering at 350 °C of unalloyed irons; however, longer treatment times led to orthorhombic η-carbides precipitation inside the plates of ferrite. They also found that ε-carbides were always present in irons austempered at 300 °C. In another publication,[15] the same authors detected precipitation of χ-carbides at the α/γ interface formed during the high carbon austenite decomposition in Al-alloyed irons austempered for more than 5 h at 400 °C. When these irons were austempered at 300 °C, ε-carbides fraction increased with time, and for 5 h of treatment χ-carbides precipitated at the α/γ interface. The ε-carbides in the austenite of Mo-Ni-Cu alloyed irons, after a 1 h of austempering treatment at 410 °C, were also reported elsewhere.[16]

The austempering treatment conditions applied in this work allowed reaction I to occur to completion; hence, the martensite was completely eliminated. Such a phase is formed when the carbon content in high carbon austenite is not enough to avoid the transformation of austenite to martensite when the material is cooled to room temperature. However, considering the simultaneity of both reactions I and II, it was impossible to avoid reaction II. Because of the chemical composition heterogeneity caused by the segregation of the alloying elements during the solidification process, the rate of reaction I was different throughout the eutectic cell. It is well known that Mn slows the

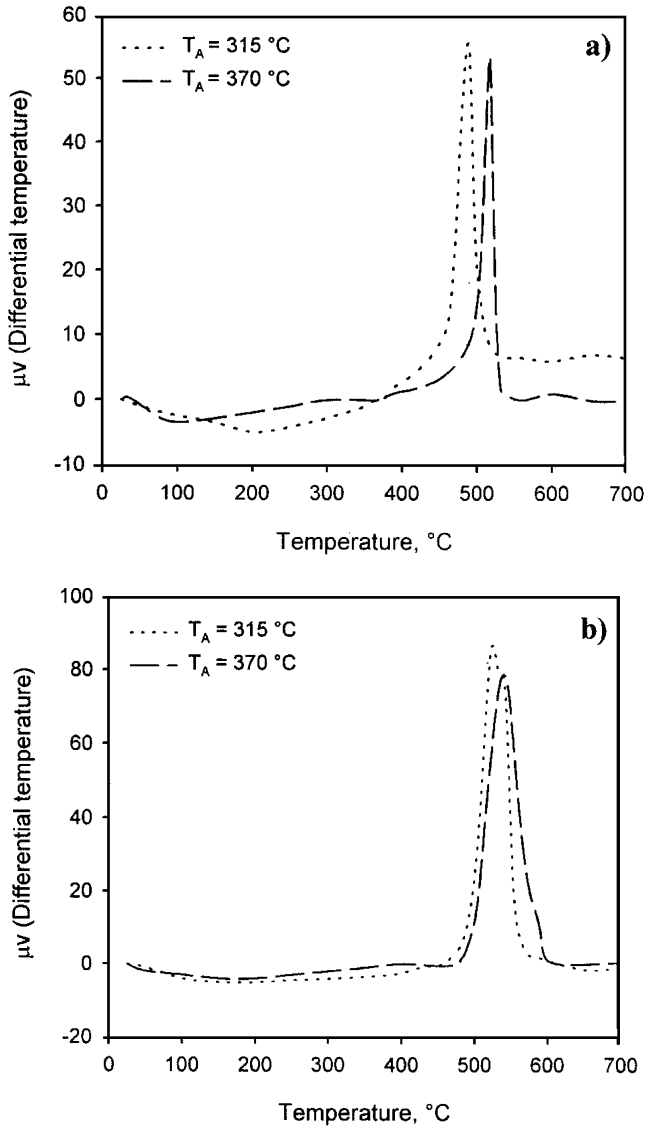

Fig. 3 DTA curves with a heating rate of 20 °C/min. **(a)** H1 austempered iron. **(b)** H2 austempered iron

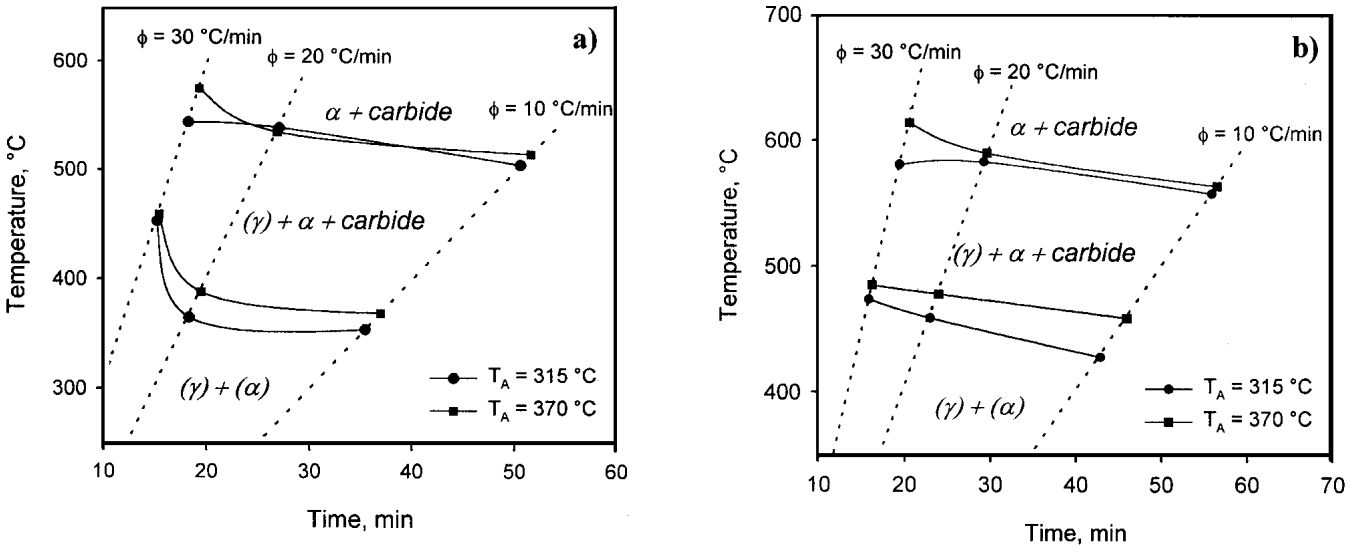

Fig. 4 High carbon austenite transformation diagrams. **(a)** H1 iron. **(b)** H2 iron

reaction rate considerably, mainly in the cell boundary where it segregates more and, consequently, the elimination of the martensite takes longer.

Table 2 resumes the carbon contents in the austenite, which was around 2 wt.%. In irons austempered at 315 °C, the carbon content was slightly lower than in those austempered at 370 °C. Nevertheless, the difference is small, and it is clear that low austempering temperature (such as 315 °C) led to a carbide precipitation that in turn decreased the available amount of carbon to be dissolved in the austenite. This table also presents the fractions of the high carbon austenite, which are higher for the highest austempering temperature. H2 iron showed a greater fraction than H1 iron.

Table 2 High Carbon Austenite Volume Fraction (X_γ) and Carbon Content (wt.%) C_γ in H1 and H2 Irons

Type of Iron	Austempering Temperature, °C	X_γ	C_γ
H1	315	0.118	2.06
	370	0.332	2.10
H2	315	0.171	2.03
	370	0.428	2.05

3.2 DTA

Figure 3 shows the DTA results for the unalloyed and Ni-Cu-Mo alloyed irons. Both kinds of iron presented a similar behavior. In the range of 0-250 °C, the small changes observed were associated to the differences in the heat capacities and the thermal conductivities between the specimen and the reference material. At higher temperatures, an exothermic peak appeared on a position that depended on the type of iron, the austempering temperature, and the heating rate. In the last part of the curve, until 700 °C, unimportant baseline changes were detected. The peak observed was related to the high carbon austenite decomposition occurring according to reaction II. In Fig. 3, the peak was shifted to higher temperatures as the austempering temperature increased. No peak was registered for unalloyed irons austempered at 420 °C because of the absence of austenite in the microstructure that consisted only of ferrite and carbides.

On the DTA curves, the onset reaction temperature, the highest reaction rate temperature, and the reaction ending temperature can be determined for the exothermic peak. Table 3 summarizes these temperature values for the three heating rates. At the heating rate of 10 °C/min, the highest thermal stability was exhibited by the alloyed iron austempered at 370 °C, and the onset of the transformation was observed at 459 °C. In contrast, the lowest stability was presented by the unalloyed iron austempered at 280 °C, in which the decomposition started at 320 °C.

Figure 4 shows the high carbon austenite transformation diagrams for the Ni-Cu-Mo alloyed and unalloyed austempered irons. The starting and ending austenite decomposition temperatures increased with the heating rate because of limited diffusion of carbon at high heating rates. The austempering temperature affects the starting more than the ending temperature of the austenite decomposition. The displacement of these curves to higher temperatures indicates that the Ni-Cu-Mo alloying elements seem to stabilize the high carbon austenite and delay the carbide precipitation.

Previous works[11] have reported the effect of the austempering time on the thermal stability of the high carbon austenite; it was found that higher carbon contents in the austenite, promoted by longer austempering time, increased the initial temperature of decomposition. The low-temperature microstructures obtained in the present work exhibited lower thermal stability, lower content carbon in the austenite, lower thickness of the ferrite and austenite plates, greater amount of ε-carbides, and lower high carbon austenite fraction. The main difference of these microstructures, with respect to those obtained at high austempering temperatures, was the thickness of the ferrite and austenite plates. Such a characteristic can be related to the interface energy that conjointly with the carbon supersaturating of the austenite lattice and the strain energy associated with

dislocations constitute the driving force for the high carbon austenite decomposition.

3.3 Microstructure Evolution During the Annealing of the H2 Iron Austempered at 315 °C

In the H2 irons austempered at 315 °C and annealed up to 300 °C, the same phases observed in the initial microstructure were found; TEM images (Fig. 5) revealed the presence of the alternating plates of ferrite and austenite, and ε-carbides located at the α/γ interface, as well as inside the ferrite plates. At 400 °C, the ε-carbide disappeared, whereas an acicular silico-carbide of triclinic structure (Fig. 6) was observed. This structure was still observed as the annealing temperature was increased up to 500 °C. In specimens annealed up to 600 °C, the only phases observed were ferrite and cementite, as shown in Fig. 7.

The precipitation of carbides with triclinic structure has been reported in bainitic Fe-Si-C alloys[17] as well as in ductile irons with prolonged austempering treatments at 410 °C.[16,18] In the latter case, it was assumed that such carbides formed from ε-carbides by a shearing mechanism. However, Hägg type monoclinic carbides were reported by Liu et al.[9] in irons aged at 360 °C for 96 h. By prolonging the aging treatment to 216 h, they observed that the monoclinic acicular carbides grew.

3.4 Microstructure Evolution During the Annealing of the H2 Iron Austempered at 370 °C

In the irons H2 austempered at 370 °C that were annealed up to 400 °C, the same phases observed in the initial microstructure were found. Fig. 8 shows the presence of ferrite, high carbon austenite, and (Fe_2C) η-carbides located inside the ferrite plates. Such carbides disappeared as the annealing temperature was increased up to 500 °C, where the microstructure comprised triclinic silico-carbides and ferrite plates. When the annealing was carried out until 600 °C, cementite precipitated and the silico-carbides disappeared.

During the nonisothermal annealing, the initial phases in the microstructure were stable up to a given temperature that depended on the austempering temperature, the chemical composition of the iron, and the heating rate. The presence of the Ni-Cu-Mo alloying elements, as well as a high austempering

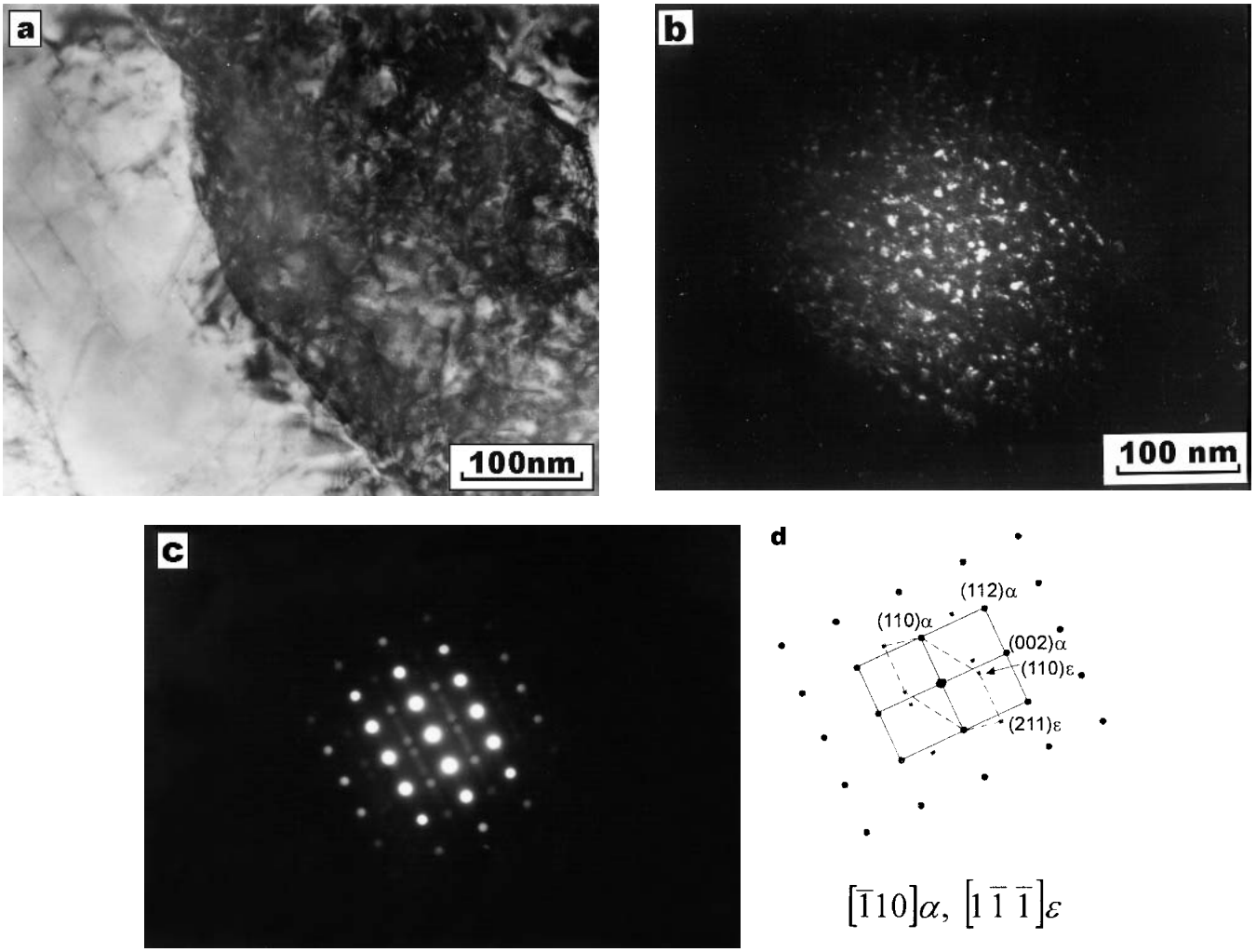

Fig. 5 TEM images of austempered (315 °C) H2 iron after the nonisothermal annealing until 300 °C. **(a)** Bright field image showing ferrite and austenite plates. **(b)** Centered dark field with (211)ε carbide reflection. **(c)** Indexed corresponding diffraction pattern

Table 3 Characteristic Temperatures of the High Carbon Austenite Transformation: Onset Temperature (T_i), Highest Reaction Rate Temperature (T_{max}), and Ending Temperature (T_f), for Different Heating Rates and Austempering Temperatures

		H1 Iron			H2 Iron		
Austempering Temperature, °C	Heating Rate, °C/min	T_i	T_{max}	T_f	T_i	T_{max}	T_f
270	10	320	459	502	383	501	547
	20	324	477	523	428	516	558
	30	445	491	536	455	525	561
315	10	354	467	505	428	509	558
	20	365	488	539	459	521	583
	30	453	502	544	474	536	581
350	10	368	478	508	457	514	561
	20	378	502	542	467	534	585
	30	458	512	574	480	553	613
370	10	369	490	515	459	520	564
	20	388	515	535	478	535	590
	30	459	525	575	485	561	614
420	10	(a)	(a)	(a)	454	516	558
	20	(a)	(a)	(a)	470	534	584
	30	(a)	(a)	(a)	474	557	610

(a) No peak was detected.

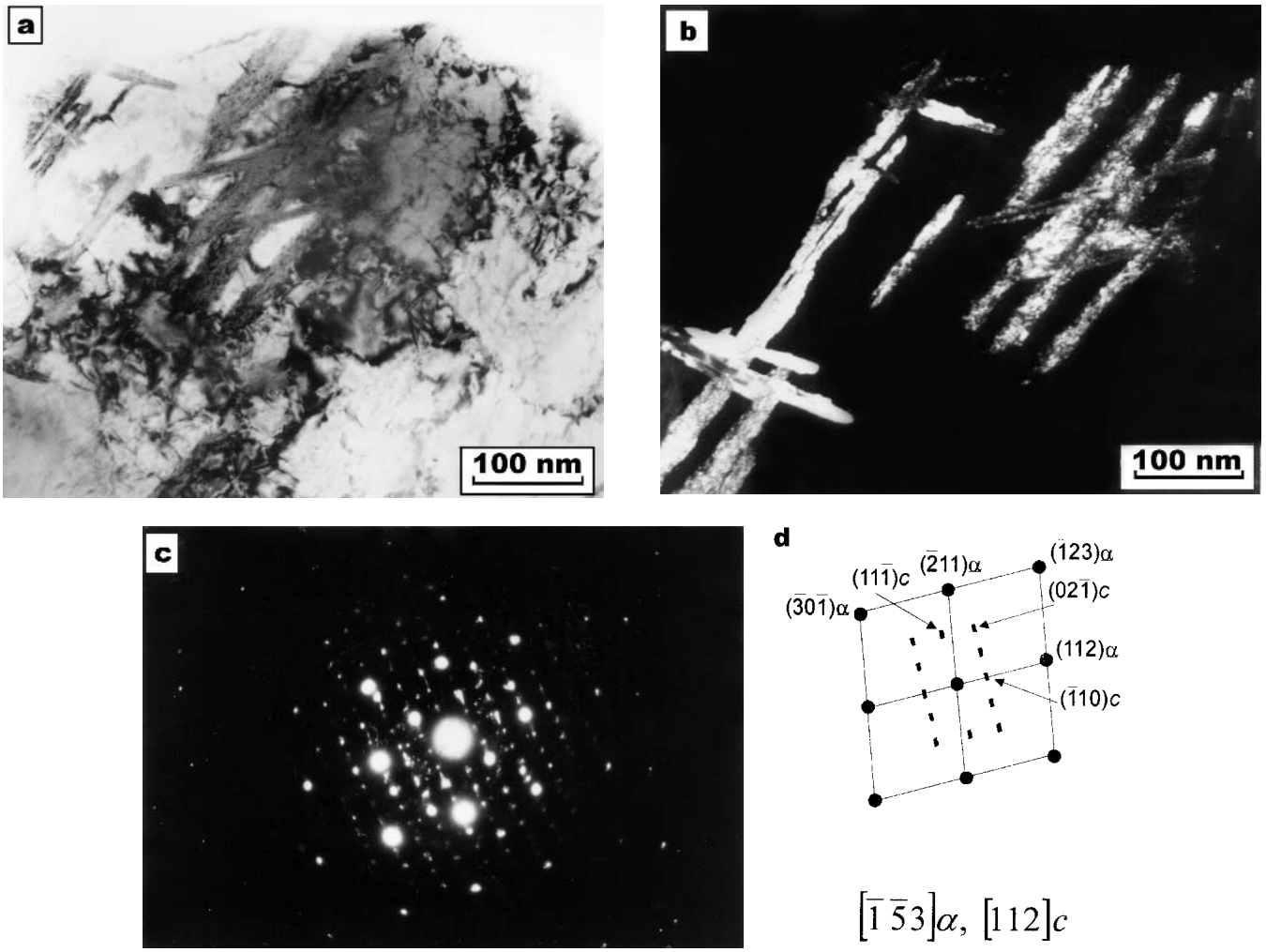

Fig. 6 TEM images of austempered (315 °C) H2 iron after the nonisothermal annealing until 400 °C. **(a)** Bright field image showing ferrite and austenite plates. **(b)** Centered dark field with (02$\bar{1}$)c triclinic silico-carbide reflection. **(c)** Indexed corresponding diffraction pattern

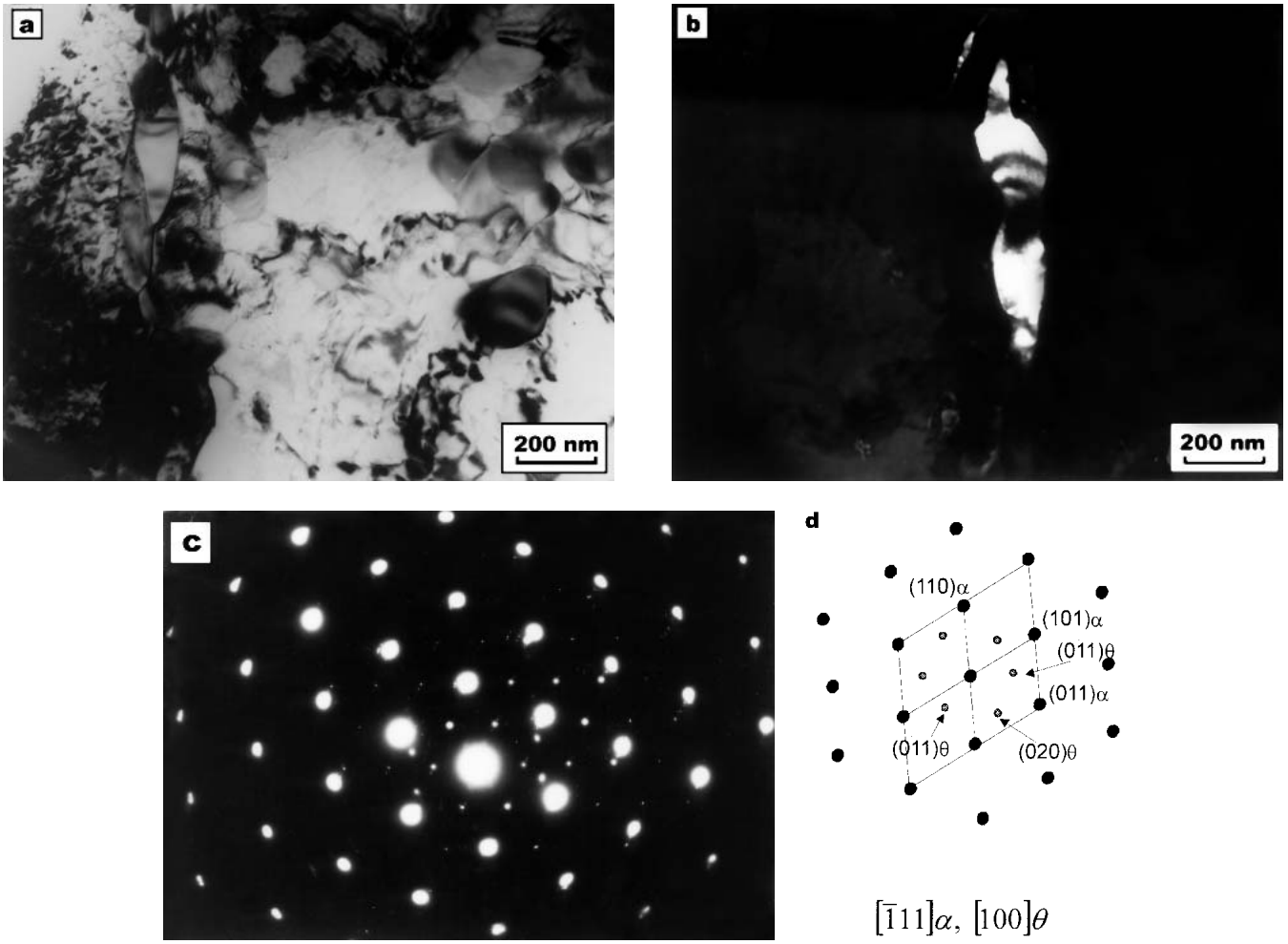

Fig. 7 TEM images of austempered (315 °C) H2 iron after the nonisothermal annealing until 600 °C. **(a)** Bright field image showing ferrite and cementite phases. **(b)** Centered dark field with $(01\bar{1})\theta$ cementite reflection. **(c)** Indexed corresponding diffraction pattern

temperature, raised the thermal stability of the high carbon austenite. Reaction II, which starts at the austempering stage, continued during the annealing treatment, increasing the amount of carbides. No changes in the DTA curves, caused by these phenomena, were observed. Conversely, the transformation of the high carbon austenite to ferrite and cementite, via the precipitation of silico-carbides, produced an exothermic peak.

4. Conclusions

From this work, which focused to study the thermal stability of the ausferritic structure during a nonisothermal annealing, the following conclusions can be drawn:

- In irons heated at a constant rate, the high carbon austenite started to decompose at higher temperatures as the austempering temperature was increased.
- The presence of the Ni-Cu-Mo alloying elements conferred a high thermal stability to ausferritic microstructure; the high carbon austenite began to decompose at higher temperatures in comparison with the unalloyed iron.
- A significant microstructural change in the austempered irons at low and high temperatures occurred above 400 and 500 °C, respectively: the high carbon austenite initiated its decomposition, precipitating triclinic structure silico-carbides. However, at 600 °C, the only exhibited phases by the microstructure were cementite and ferrite.

References

1. D.J. Moore, T.N. Rouns, and K.B. Rundman: "The Relationship Between Microstructure and Tensile Properties in Austempered Ductile Irons," *AFS Trans.*, 1987, *95,* pp. 765-74.
2. N. Darwish and R. Elliot: "Austempering of Low Manganese Ductile Irons Part 3: Variation of Mechanical Properties With Heat Treatment Conditions," *Mater. Sci. Technol.*, 9, 1993, pp. 882-89.
3. A.S. Hamid Ali and R. Elliot: "Austempering of a Mn-Mo-Cu Alloyed Ductile Iron, Part 2: Structure Mechanical Property Relationships," *Mater. Sci. Technol.*, 1996, *12,* pp. 780-87.
4. R. Elliot: "The Role of Research in Promoting Austempered Ductile Iron," *Heat Treat. Met.*, 1997, *3,* pp. 55-59.
5. D.J. Moore, T.N. Rouns, and K.B. Rundman: "Effect of Manganese on

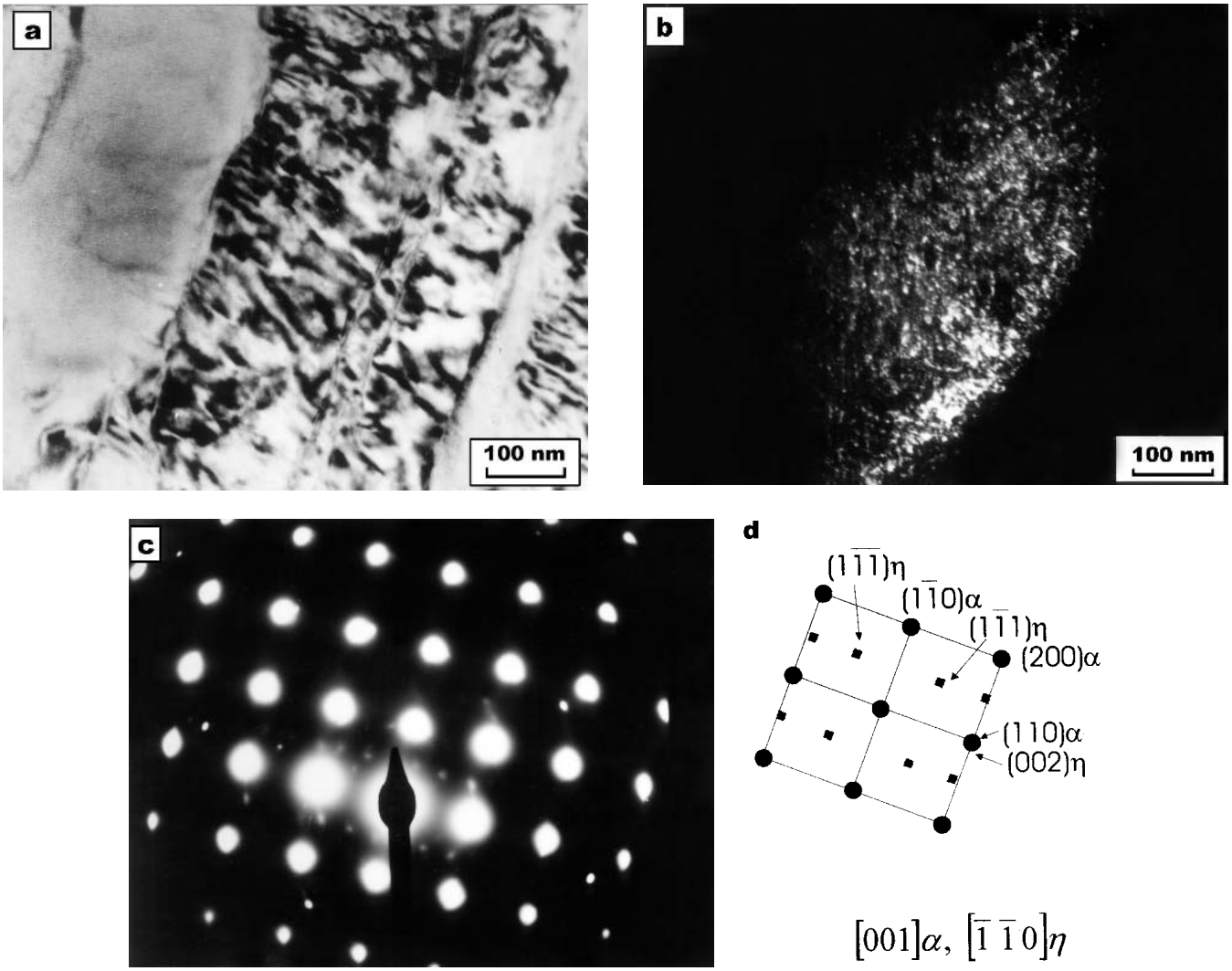

Fig. 8 TEM images of austempered (370 °C) H2 iron after the nonisothermal annealing until 400 °C. **(a)** Bright field image showing ferrite and austenite plates. **(b)** Centered dark field with $(1\bar{1}\bar{1})\eta$ carbide reflection. **(c)** Indexed corresponding diffraction pattern

Structure and Properties of Austempered Ductile Iron—A Processing Window Concept," *AFS Trans.*, 1986, *94,* pp. 255-64.

6. A. Nazarboland and R. Elliot: "The Relationship Between Austempering Parameters Microstructure and Mechanical Properties in a Mo-Mn-Cu Alloyed Ductile Iron," *Int. J. Cast. Met. Res.*, 1997, *9,* pp. 295-308.
7. S. Yazdani and R. Elliot: "Influence of Molybdenum on Austempering Behavior of Ductile Iron: Part I," *Mater. Sci. Technol.*, 1999, *5,* pp. 531-40.
8. J.P. Chobaut, P. Brenot, and J.M. Schissler: "Secondary Martensite Formation During the Tempering of Bainite S.G. Cast Irons," *AFS Trans.*, 1988, *88,* pp. 475-80.
9. Y.C. Liu, J.M. Schissler, J.P. Chobaut, and H. Vetters: "Study of the Structural Evolution of Austempered Ductile Iron (ADI) During Tempering at 360 °C," *Metall. Sci. Technol.*, 1995, *13*(1), pp. 12-20.
10. J.M. Massone, R.E. Boeri, and J.A. Sikora: "Decomposition of High-Carbon Austenite in ADI," *AFS Trans.*, 1996, *104,* pp. 133-37.
11. S. Korichi and R. Priestner: "High Temperature Decomposition of Austempered Microstructures in Spheroidal Graphite Cast Iron," *Mater. Sci. Technol.*, 1995, *11,* pp. 901-07.
12. G. Nadkarni and S. Gokhale: "Elevated Temperature Microstructural Stability of Austempered Ductile Irons," *AFS Trans.*, 1996, *104,* pp. 985-94.
13. B.D. Cullity: *Elements of X-ray Diffraction,* Addison-Wesley, Reading, MA, 1987.
14. L. Sidjanin and R.E. Smallman: "Metallography of Bainitic Transformation in Austempered Ductile Iron," *Mater. Sci. Technol.*, 1992, *8,* pp. 1095-1103.
15. L. Sidjanin, R.E. Smallman, and J.M. Youns: "Electron Microstructure and Mechanical Properties of Silicon and Aluminium Ductile Irons," *Acta Metall. Mater.,* 1994, *42,* pp. 3149-56.
16. J. Aranzabal, I. Gutierrez, and J.J. Urcola: "Influence of Heat Treatments on Microstructure of Austempered Ductile Iron," *Mater. Sci. Technol.*, 1994, *10,* pp. 728-37.
17. B.P.J. Sandvik: "The Bainite Reaction in Fe-Si-C Alloys: The Primary Stage," *Metall. Trans. A*, 1982, *13A,* pp. 777-87.
18. I. Gutierrez, J. Aranzabal, F. Castro, and J.J. Urcola: "Homogeneous Formation of Epsilon Carbides Within the Austenite During the Isothermal Transformation of a Ductile Iron at 410°C," *Metall. Mater. Trans. A*, 1995, *26A,* pp. 1045-60.